Proceedings of ASME Turbo Expo 2011
GT2011
June 6-10, 2011, Vancouver, British Columbia, Canada

GT2011-45460

IMPROVEMENT OF OXIDE/OXIDE CMC AND DEVELOPMENT OF COMBUSTOR AND TURBINE COMPONENTS IN THE HIPOC PROGRAM

Miklós Gerendás &
Yannick Cadoret
Rolls Royce Deutschland Ltd & Co KG
Dahlewitz, Blankenfelde-Mahlow, Germany

Christian Wilhelmi &
Thays Machry
EADS Innovation Works
Munich, Germany

Ralf Knoche
ASTRIUM Space Transportation
Bremen, Germany

Thomas Behrendt &
Thomas Aumeier
German Aerospace Center (DLR): Institute of Propulsion Technology (AT), Cologne, Germany

Sandrine Denis
German Aerospace Center (DLR): Institute of Structures and Design (BK), Stuttgart, Germany

Jürgen Göring
German Aerospace Center (DLR): Institute of Materials Research (WF), Cologne, Germany

Dietmar Koch &
Kamen Tushtev
Advanced Ceramics, University of Bremen, Bremen, Germany

ABSTRACT
Three different oxide/oxide ceramic matrix composite (CMC) materials are described. Design concepts for the attachment of the CMC component to the metal structure of the gas turbine are developed in a first work stream focused on the combustion chamber and the turbine seal segment. Issues like environmental barrier coating (EBC)/thermal barrier coatings (TBC), application and volatilization, allowance for the different thermal expansion and the mechanical fixation are addressed. The design work is accompanied by CFD and FEM simulations. A variation of the microstructural design of the three oxide/oxide CMC materials in terms of different fiber architecture and processing of matrix are considered. Also, mechanical properties of these variations are evaluated. The material concepts are developed further in a second work stream. The CMCs are tested in various loading modes (tension, compression, shear, off-axis loading) from room temperature to maximum application temperature focusing on tensile creep behavior. By modification of the matrix and the fiber-matrix interface as well as EBC coatings, the high temperature stability and the insulation performance are enhanced. An outline of the "High Performance Oxide Ceramic"-program HiPOC for the following years is given, including manufacturing of a high-pressure tubular combustor and turbine seal segments from the improved materials as technology samples, for which validation testing up to technology readiness level 4 is scheduled for 2011.

INTRODUCTION
In the framework of the 3 year collaborative German national funded HiPOC program started February 2009, three different oxide/oxide CMC materials are developed, which may be used in gas turbines for power generation and aerospace propulsion, or as spin-off in space applications. The aim is, in conjunction with an improved thermal management, to minimize the fuel consumption and thereby reduce the CO_2 emission from the gas turbine. To achieve this goal, design concepts for the attachment of the CMC component to the metal structure of the engine are developed in a first work stream focused on the combustion chamber and the turbine seal segment. Issues like EBC/TBC application and volatilization, allowance for the different thermal expansion and the mechanical fixation are addressed. The design work is accompanied by computational fluid dynamics (CFD) and finite element method (FEM) based simulations. A variation of the microstructural design of the three CMC materials in terms of different fiber architecture and processing of matrix are considered. To enhance the required thermo-mechanical properties and long-term stability of the components, the material concepts are developed further in a second work stream and validated by material testing. By modification of the matrix and the fiber-matrix interface as well as EBC coatings, the high temperature stability and the insulation performance are enhanced. As for precise simulations

detailed experimental data are necessary, the oxide/oxide CMC are tested in various loading modes (tension, compression, shear, off-axis loading) from room temperature to maximum application temperature. These studies indicate the high temperature potential of the CMC materials under investigation and support the development of thermal and mechanical design rules.

1. MATERIAL DEVELOPMENT

Ceramic materials generally display excellent temperature stability, high hardness and good corrosion and erosion resistance. To achieve damage-tolerant and favorable failure behavior reinforcing components such as particles [1], whiskers or chopped fibers [2] and continuous fibers were employed, the latter being most promising [3]. Ceramics such as nitrides, carbides, borides or carbon achieve high strength and excellent creep resistance up to elevated temperatures which is due to their predominant covalent bonding. The fundamental drawback of these materials, however, is their susceptibility to oxidation. Thus, for many years every endeavor has been made to extend the lifetime of non-oxide materials by protective coatings [4,5]. Long-term oxidation protection, however, is hard to obtain, particularly when the coated composites are used under cyclic thermal or mechanical load. As a consequence, there is an increasing interest in oxide fiber/oxide matrix ceramics (oxide/oxide CMCs) as structural materials for high temperature applications in oxidizing atmosphere [5].

1.1 WHIPOX

Oxide/oxide CMC's with porous matrices without interface between fibers and ceramic matrices have been developed since the mid 1990´s [6]. The porous matrices typically consist of alumina or aluminum silicates. The bonding between a porous matrix and the incorporated fibers typically is weak, thus leading to matrix crack deflection along the fiber/matrix interface. Moreover, the matrix strength is strong enough to allow stress transfer between the fibers and the single layers. Costly fiber coatings and elaborate matrix densification techniques are not required.
The oxide/oxide composites at DLR (WHIPOX = Wound Highly Porous Oxide Matrix CMC) [7] are manufactured by filament winding. The fibers used are commercial Nextel 610 fibers, fabricated by 3M, St. Paul, MN (USA) in a pure alumina matrix. The matrix is derived from a commercial pseudo-boehmite/amorphous silica phase assemblage with overall compositions ranging between 70 and 100wt-% Al_2O_3. The processing route is shown schematically in Fig. 1. In a first step the organic fiber sizing of the continuous fibers is removed by thermal decomposition in a tube furnace. The cleaned fiber tow is continuously infiltrated with a water-based matrix slurry. Then the infiltrated tow is pre-dried in order to stabilize the matrix and finally wound in 1D-2D orientation on a mandrel.

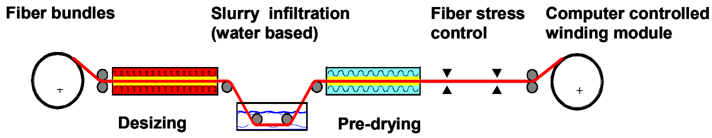

Fig. 1: Schematic fabrication steps of WHIPOX CMC's

Green bodies are removed from the mandrel in the moist stage which allows subsequent stacking, forming or joining of the prepregs. Once in their final shapes, the green bodies are sintered free-standing in air at ~1570K. High porosity allows easy mechanical finishing of sintered WHIPOX CMCs. Conventional machining methods (drilling, cutting, grinding, milling etc.) can be applied. Fiber contents of WHIPOX CMCs range between 25 and 50 vol-%.
Nextel 610 is a fiber consisting of single phase α-alumina with an average grain size of ~80nm. The fiber tows used for the winding process consist of about 800 single filaments with a diameter of 12µm. The fiber orientation in the CMC was chosen to ± 30° or ± 60° depending on loading direction. The fiber content was 37vol-%, the density 2,82g/cm^3, the matrix porosity 46% and the total porosity 28%.

1.2 UMOX™

UMOX™ is the standard oxide based CMC used at EADS Innovation Works. It was developed during the last 20 years and already successfully flight tested with a Do 228 aircraft jet engine equipped with exhaust components.
For a specific type of the UMOX™ material, the matrix is based on a commercial micron-sized mullite powder and polysiloxane precursor. Continuous alumina fibers of type Nextel 610 were used as reinforcement fibers. In order to conform to the criterion for a weak fiber-matrix interface preventing propagation of cracks through the fibers, materials with a dense matrix need an engineered debond region between the fiber and the matrix. This allows cracks to be deflected along the fiber/matrix interface, leaving a smooth path to allow fiber pull-out. For this reason a gap between fiber and matrix is generated by using an organic fiber coating, which is removed after composite manufacture (fugitive interface) [8, 9].
The oxide CMC is manufactured by the PIP (Polymer Infiltration Pyrolysis) process. With this technique, coated oxide fibers are infiltrated with liquid pre-ceramic matrix slurry (Liquid Polymer Infiltration, LPI) and wound onto a constantly rotating drum or mandrel (up to 1.5 m in diameter). The unidirectional lay-up of the impregnated fiber bundles in each layer is realized by continuous working fully automated 6+2 axis robot controlled filament winding process allowing high flexibility in fiber architectures with various fiber orientations and geometrical shapes with the feasibility of integral structure design. In Figure 2, a schematic flowchart of the PIP process for the manufacture of UMOX™ at EADS is illustrated [10].

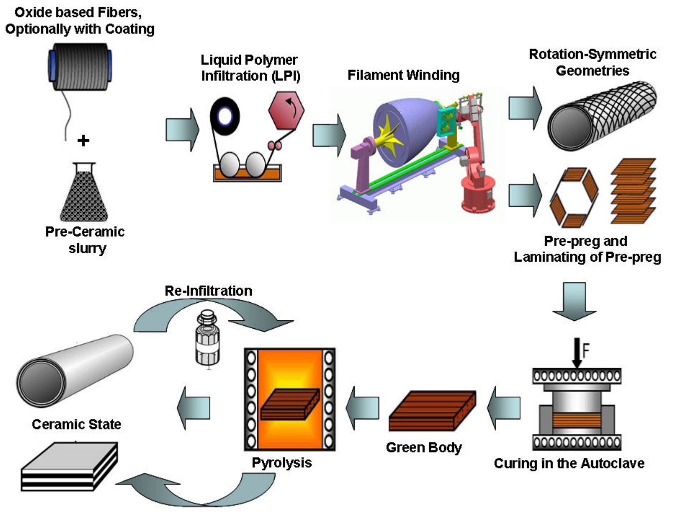

Fig. 2: Manufacturing process for UMOX™: Schematic flowchart of the PIP process [10]

After drying the impregnated fibers are vacuum packed and consolidated in an autoclave process under >10 bar pressure at T>423K. The polymer in the matrix forms a cross-linked network at this temperature to bond the laminate together and give a green body that is solid enough for handling and further processing. Following, the pre-ceramic matrix is converted to a ceramic by pyrolysis in an inert atmosphere at temperatures above 1270K. Shrinkage of the pre-ceramic matrix during pyrolysis leaves some porosity in the material. Re-infiltration cycles of the composite with a polymeric precursor followed by further high temperature treatment reduce the open porosity. The number of re-infiltration cycles depends on the desired material porosity and properties [11]. A typical fiber volume content of the described CMC material with outstanding mechanical and thermo-mechanical properties is 48-50vol-% with 10-12vol-% porosity and density of 2.4-2.5g/cm^3.

1.3 OXIPOL®

In the scope of the HiPOC program, the DLR Institute of Structures and Design is further developing its oxidic CMC based on polymers (OXIPOL). OXIPOL is built up by oxide ceramic fabrics and a SiOC matrix derived from polysiloxane precursors [12]. Near net-shape manufacture of complex shaped components is achieved via a new PIP route (polymer infiltration and pyrolysis, Figure 3). A high damage tolerance is guaranteed via fugitive coating, which weakens the fiber/matrix interface.

In a first step of the OXIPOL manufacturing, the oxide fabrics, sized or desized, are coated with a phenolic resin (JK60) dissolved in ethanol, in a Foulard machine. The coated fabrics are then subsequently dried at room temperature and cured at 448K for 2 h.

The matrix is consolidated via warm pressing method. By this method, dried fabric sheets and layers of resin powder (MK, Wacker Chemie) were stacked up to a laminate and warm pressed. Thereby, the fabrics were infiltrated with the polymer, which was cured under axial load and at low pressure (50mbar). For the following densification steps, the pyrolysed preform was then plunged in a liquid polysiloxane precursor (50 mass-% MSE100 and 50 mass-% MK, Wacker Chemie) assisted by near-vacuum. In order to obtain a relatively dense material with an open porosity of approximately 10 vol.-%, five PIP cycles were used. Typical fibre volume content was about 42.5 %.

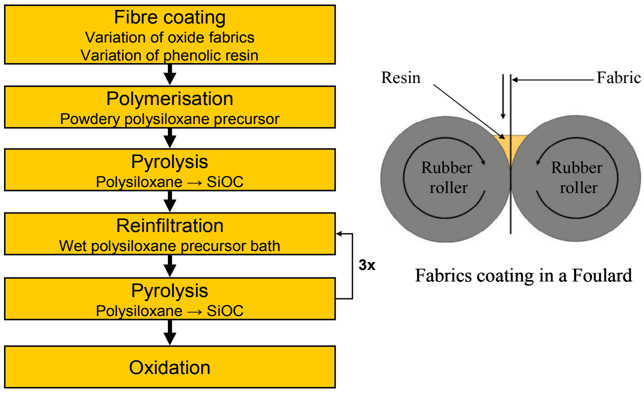

Fig. 3: PIP process used to manufacture OXIPOL

After finishing the matrix, built up via PIP cycles, the OXIPOL plates are oxidized at 973K for 20 h in air, leading to a gap between the fibers and the matrix. Within 12 months, 15 variations of fugitive coatings and oxide fabrics were investigated. The following three different kinds of oxidic fabrics were used:

a.) Plain weaves based on alumina silicate fibers (fibers: Nitivy Alf 72/28, fabrics 2626P, Nitivy Co., LTD),
b.) 8 harness satin weaves based on
 i.) alumina fibers (fibers Nextel 610, fabrics DF-19, 3M) and
 ii.) mullite fibers (fibers Nextel 720, fabrics XN-625, 3M).

For each kind of fabric, five variations of fiber coatings were investigated (table 1):

Type & mass-%	A	B	C	D	E
Phenolic resin content JK60	0	10	10	5	5
Coating cycles	0	1	2	2	2
Pyrolysis cycles	0	0	0	0	1

Table 1. Coating parameters for the investigated fabrics

Open porosities and densities of each 15 OXIPOL plates were determined by Archimedes method (DIN EN 993-1) after each pyrolysis and oxidation step. Tensile properties before and after thermal exposure at 1470K in air were determined acc. to DIN EN 658-1 [13]. Three-point bending properties were characterised before and after thermal exposure at 1273K and

1473K in air acc. to DIN EN 658-3. Additionally, the microstructures of the coated fabrics, the CMC plates and the fracture surfaces were analyzed via SEM (Scanning Electron Microscopy). Quality of the plates was assessed via air-coupled ultrasound or computer tomography techniques.

Figure 4 summarizes the tensile strength results before and after exposure at 1473K in air. The OXIPOL configuration based on Nextel 610 fabrics showed the highest tensile strength of up to 134MPa. The coating process influenced strongly the tensile strength. A tensile strength improvement was obtained with several coatings with lower resin concentration and an intermediate pyrolysis of the coated fabrics. Compared to the uncoated configuration Nextel 610, the two times coated configuration with 5% phenolic resin solution and an intermediate pyrolysis presented a 3.6 times higher tensile strength.

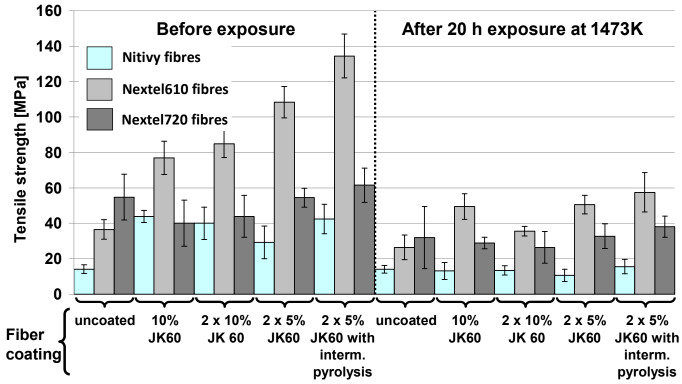

Fig. 4: Tensile strengths of OXIPOL based on three different fabrics and five different coatings

Despite all improvements of the mechanical properties before exposure, tensile properties degraded strongly after exposure at 1473K in air. Due to the growth of the matrix (oxidation reactions), the gap between fibers and matrix closed itself. This leads to a decrease of all tensile strengths at levels close to those of the uncoated OXIPOL versions.

1.4 Material testing

The mechanical characterization of the different types of composites, was conducted at room temperature in four loading modes: tension, compression, in-plane shear and four-point bending. The tests were performed on universal testing machines (Zwick 1465, Zwick Z005) under quasi-static condition with constant loading rate of 1 mm/min. Dog-bone specimens for the tensile and rectangular specimens for compression and four-point bending tests were used. The in-plane shear tests were performed on double-notched Iosipescu specimens. The orthogonal reinforced composites UMOX and OXIPOL were tested under tensile and compressive loading in fiber (on-axis) and 45° to the fiber (off-axis) directions. For shear and four-point bending only on-axis tests were performed. WHIPOX-specimens were tested with +30°/-30° and +60°/-60° fiber orientation to the loading direction, only. For each type of test, three identical specimens were tested.

Tensile strain was measured with a laser based contactless strain measurement system (Fiedler, Germany) and a biaxial clip-on extensometer (MTS). In compression and shear tests strain was evaluated from strain gauges. An inductive displacement transducer was used for measurement of deflection of specimens in four-point bending mode. The following section details the experimental results.

1.4.1 Tensile mode

UMOX and OXIPOL present an almost linear behavior up to failure with relatively high stiffness and strength in on-axis loading (Fig. 5). In this case, fibers oriented in loading direction provide a direct load transfer between the grips of the testing machine. The transverse strain of both composites is very low as the transversely oriented fibers prevent larger strains.

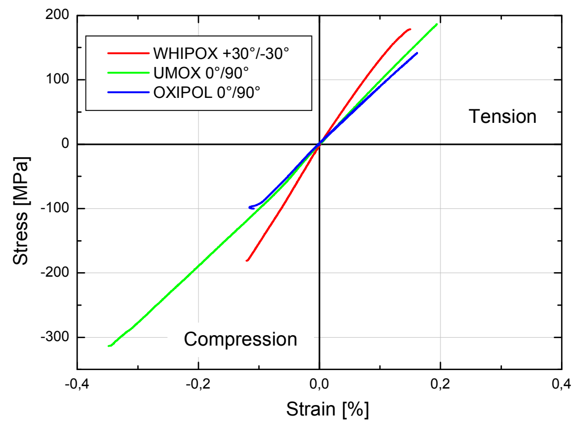

Fig. 5: Representative stress-strain curves of the tree tested composites under tensile and compressive mode

WHIPOX behaves almost linear elastic under tensile loading in +30°/-30° orientation (Fig. 5). While strength is comparable to UMOX and OXIPOL (Fig. 7), the stiffness is about 30 % higher (Fig. 6). Due to tensile loading in +30°/-30° orientation, all fibers are able to carry load even if no direct load transfer of fibers can be achieved between the grips of the testing machine. This also indicates that the matrix is able to transfer the applied load to the slightly off-axis oriented fibers. In case of +60°/-60° fiber orientation, the matrix has to carry most of the load which results in a strongly reduced composite stiffness (Fig. 8). Due to the small width of the specimens failure occurs at very low stress level without fiber failure (Fig. 9).

Also in case of UMOX and OXIPOL, the stiffness in off-axis loading (Fig. 8) is much lower compared to on-axis loading (Fig. 6). The even lower stiffness compared to WHIPOX indicates weaker matrices in case of UMOX and OXIPOL. These weak matrix properties lead to nonlinear stress-strain behavior and large axial and transverse deformations (about 0,4%) up to failure.

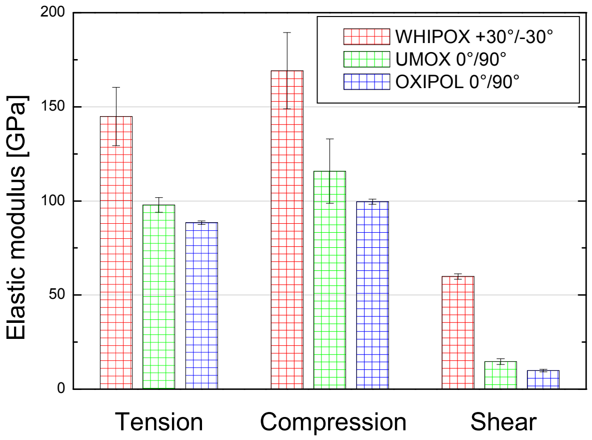

Fig. 6: Elastic moduli of composites with different fibre reinforcement under tensile, compressive and shear modes

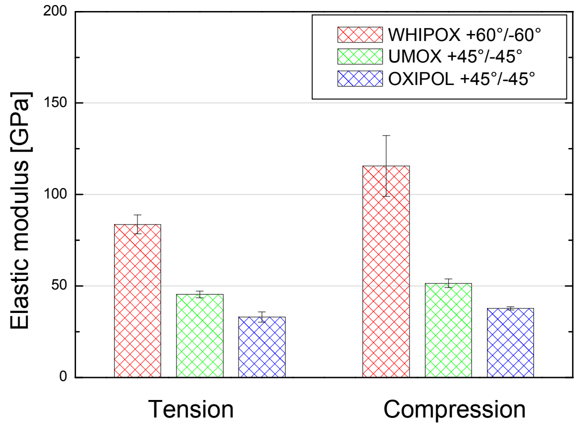

Fig. 8: Elastic moduli of composites with different fibre reinforcement under tensile, compressive and shear modes

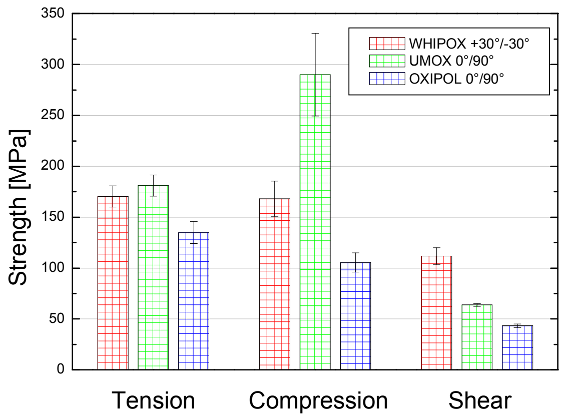

Fig. 7: Strength of composites with different fibre reinforcement under tensile, compressive and shear modes

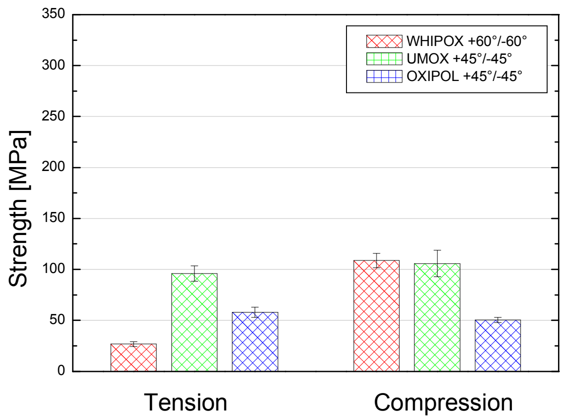

Fig. 9: Strength of composites with different fibre reinforcement under tensile, compressive and shear modes

The slightly lower stiffness and strength of OXIPOL compared to UMOX composite in both 0° and 45° directions can be explained by fiber undulations and a weaker matrix.

For on-axis loading, ultimate composite failure occurs when the fiber strength is reached while failure emerges locally within the gauge length (Fig. 7). Only in case of OXIPOL moderate fiber-bundle debonding occurs. Under off-axis loading all tested composites fail localized in the gauge area as the failure processes are initiated by the shear stresses along the fiber and the fracture surface is dominated by the fiber orientation (Fig. 9). In case of WHIPOX, additionally out-of-plane shear failure is observed.

1.4.2 Compressive mode

Under both on-axis and off-axis compressive loading the mechanical behavior of all tested composites is almost linear elastic (Fig. 5) and final failure mechanisms are contributed to fiber buckling and shear failure.

All specimens loaded in fiber direction have a higher stiffness and strength (Fig. 6 & 7) than the off-axis specimens (Fig 8 & 9) due to the higher stiffness of fibers compared to the stiffness of matrix. In comparison to tensile stiffness, the compressive stiffness is even higher as the pre-existing matrix cracks are closed under compression. UD cross-ply lay-up and straight orientation of the fibers of UMOX results in a significantly higher strength compared to woven or fabric structures of WHIPOX and OXIPOL as the fiber undulations tend to bend easier compared to straight oriented fibers and the weak matrix is not able to prevent fiber buckling. In case of off-axis loading superimposed shear stresses additionally reduce the compressive strength (Fig. 9).

1.4.3 Shear mode

The in-plane shear behavior of the orthogonal reinforced composites UMOX and OXIPOL is considerably non-linear (Fig. 10). Matrix damage occurs already at low stresses resulting in a reduced stiffness of the composites and large shear deformation (more than 2%) up to ultimate composite failure. Because of better matrix properties UMOX exhibits higher stiffness and strength compared to OXIPOL. All tested specimens failed in shear mode between the notches.

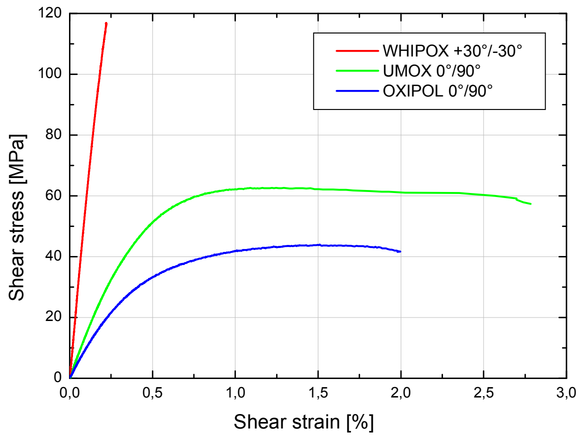

Fig. 10: Representative stress-strain curves of the composites under shear mode

In contrast, the filament wound composite WHIPOX with +30°/-30° reinforcement is less sensitive to shear loading as the fibers prevent failure in the shear zone. Thus, valid shear strength value could not be achieved as all specimens failed locally in the grips region, where high compressive stresses occurred. Up to maximum applicable load the shear stress-strain curve is linear elastic (Fig. 10) with shear modulus more than four times higher compared to the two other composites.

1.4.4 Four-point bending (interlaminar shear properties)

For all composites load versus deflection curves are linear indicating elastic material deformation. Beyond maximum load successive interlaminar shear failure was observed in all cases while WHIPOX exhibited the best interlaminar properties due to the highest matrix strength (Fig. 11).

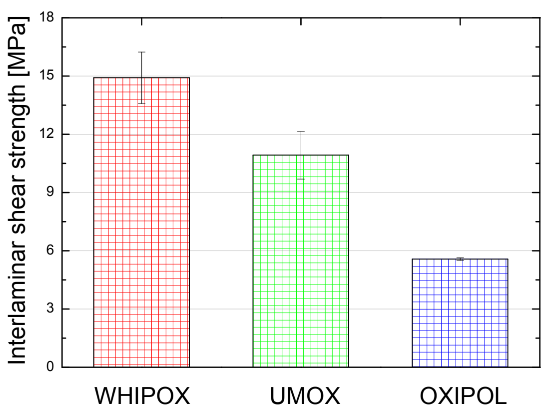

Fig. 11: Interlaminar shear strength obtained by four-point bending test

1.5 Abradable EBC Coating

An EBC is required to protect the CMC against water vapor attack, as the partial pressure can reach 10% of the gas pressure resulting in 5bar water vapor partial pressure in large civil engine with an overall pressure ratio of 50. The development of the EBC for the ox/ox CMC under evaluation is carried out at the Forschungszentrum Jülich GmbH, Institut für Energieforschung IEF-1, Jülich, Germany, as there is experience with the development of advanced and abradable APS coatings [14-16]. Three coating systems have been studied: Partially yttrium stabilized zirkonia (YSZ, as reference), magnesium spinel [16] and a binary system mullite + rare earth mono-silicate. The WHIPOX samples were first coated by a reaction bonded alumina layer to provide a better interface for the coating resulting in a smooth surface. All samples were prepared by a slight sandblasting. The air plasma sprayed (APS) EBC was applied using standard Triplex Pro 200 equipment. The thickness was 0,6mm. The YSZ coating was rather dense, and the spinel as well as the silicate coating rather porous. A cyclic burner rig with compressed air for back-side cooling was used for a quick evaluation and ranking of the different coatings [15]. The samples were heated for 5 minutes to 1723K coating surface temperature measured by pyrometer and 1323K average CMC temperature measured by thermocouple in the center of the 30mm coupon followed by a forced cooling period of 2 minutes to reach room temperature. The resulting number of cycles to spallation for a single coupon is displayed in Fig. 12.

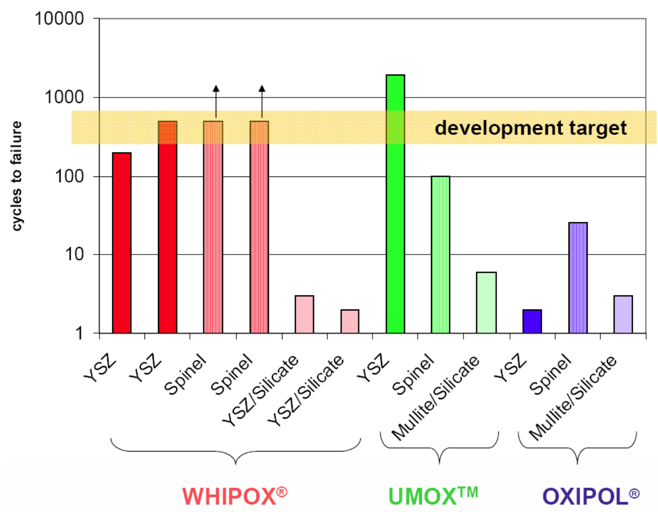

Fig. 12: Coating thermal cycling results

On WHIPOX, both YSZ and spinel reached the development target for this specific rig and its conditions of 500 cycles. Two spinel coated WHIPOX coupons were cycled further and finally failed at 1515 and 1705 cycles, respectively. The YSZ coating on UMOX spalled after 1921 cycles, a surprisingly long life for a rather dense coating. The other combinations of coating and substrate, especially in conjunction with OXIPOL, did not perform well indicating, that the surface preparation and the spraying parameter did not result in a suitable bond between CMC substrate and APS coating. Further analysis of the results will be carried out in order to understand the performance of the coating. Based on the outcome, an optimization will be carried out especially on the low-life combinations with the remaining duration of the program. The promising combinations will be tested for their abradability to ensure a good cut of the blade into the coating without damage of the blade tip as this is required to perform the function of an abradable coating on a turbine sealing segment. Thermo-gravimetric measurements will be carried out to evaluate CMC and EBC sensitivity to water vapor corrosion and oxidation. Also manufacturing trials on laser drilling through EBC-coated CMC specimens will be conducted as this is the envisioned manufacturing route for the combustion chamber described below.

2. COMPONENT DEVELOPMENT

During the initiation of the HiPOC program, several gas turbine components in the hot section were studied for their potential improvement by CMC application, such as combustor, blades & vanes in the high pressure and low pressure turbine as well as seal segments/turbine liners/blade tracks throughout the engine and exhaust components. By comparing the initial material capability and the operating environment of the individual components, but also taking the customer benefit into account, the combustor and the HP turbine seal segment were selected as applications for the CMCs under development in this program.

2.1 Combustor

Combustor wall development and testing is done at different levels of abstraction (TRL technology readiness level). In a first step, planar wall elements are developed and tested at realistic engine conditions. These CMC wall elements have cooling holes and may have a TBC/EBC, but they do not have any CMC-specific mounting concept. A tubular combustor developed in a second step additionally has a CMC-specific mounting concept. The combustor will be tested at real engine conditions in an existing rig made from metallic alloys. The CMC components, with relatively low coefficient of thermal expansion compared to metallic alloys, will be fitted in this test bench. During operation, the differences in thermal expansion between the CMC and metallic components can lead to failure of the CMC components.

This tubular CMC combustor is developed as segmented or one-piece design. The one-piece design might ease manufacturing of the combustor tube itself. The segmented design would allow better access to the hot surface for cooling hole manufacturing and EBC application and all three CMCs could be tested at the same time, which saves substantial rig operating cost. But the complexity of the combustor design is increased. The CMC combustor will be tested in a rig similar to the combustor rig described in [17].

2.1.1 Tubular design

ASTRIUM Space Transportation focuses on the tubular design of the combustion chamber including its mechanical attachment system. Thereby the design has to meet various requirements which mainly can be broken down to geometrical boundary condition of the test rig, the lifetime performance under severe thermo-mechanical loading conditions as well as displacement limitation and stiffness requirements. The design is further influenced by manufacturing capabilities and experiences in advanced CMC fabrication which, in case of the tubular design, is tailored to the UMOX^{TM} manufacturing process. Additional design drivers can emerge from the development outcomes of the other disciplines such as within material and EBC developments as well as optimized cooling configurations.

The challenging requirements, but especially the strong interaction between them, require an iterative designing process accounting for e.g. manufacturing experiences, CMC adequate design know-how, and FEM analysis capabilities in order to verify the feasibility of the intended design. Similar approaches and challenges as for gas turbine combustion chambers have already been encountered by ASTRIUM Space Transportation, however, during developments of Hot Structures (HS) and Thermal Protection Systems (TPS) for (reusable) re-entry vehicles. The experiences gained over many years within CMC technology for HS & TPS (such as for X-38, PARES, or IXV Nose Assembly [18-22]) is transferred to the specific gas turbine environment and tailored to corresponding requirements and boundary conditions.

Several design concepts have been established within the project and are constantly refined with further findings and results. Currently two tubular combustion chamber concepts are analyzed in detail, which are presented in Figure 13 and Figure 14. A metallic spring attachment scheme is used to mount the liner, less stiff than the arrangement used in [23]. The upstream spring attachment accounts for the difference in radial expansion between metal casing and CMC liner. The axial location against the front seal is ensured by a leaf spring at the downstream end of the combustor in conjunction the pressure difference across the CMC combustion liner pushing in the same direction. Figure 13a shows the tubular combustion chamber in an assembled state within the pressurized casing of the test rig, whereas Figure 13b shows the oxide CMC combustion chamber with its attachment system without the casing. Special attention has to be given to the attachment system, since the right balance between flexibility (decreasing the thermally induced stresses) and stiffness (accounting for allowable displacements and frequency requirements) has to be achieved.

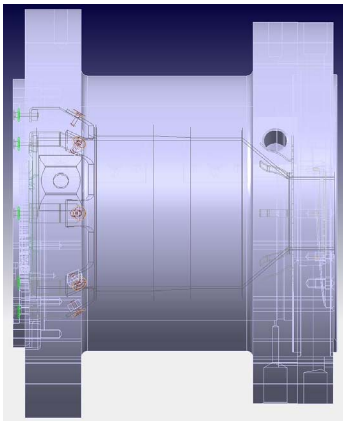

Fig. 13a: Tubular combustion chamber design C 3-1 including attachment systems in assembled state within the test rig

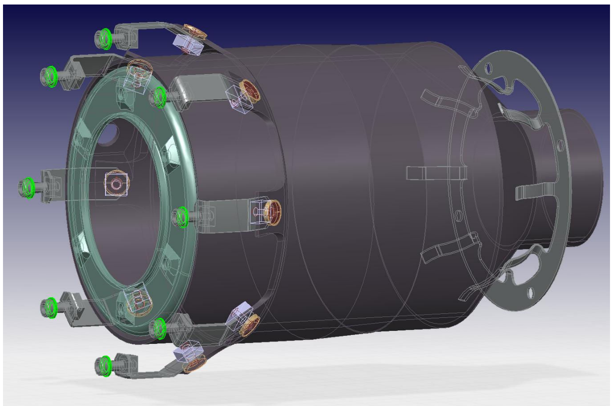

Fig. 13b: Tubular combustion chamber design C 3-1 including attachment systems showing the upstream integral CMC/metallic attachment system and the rear metallic spring element

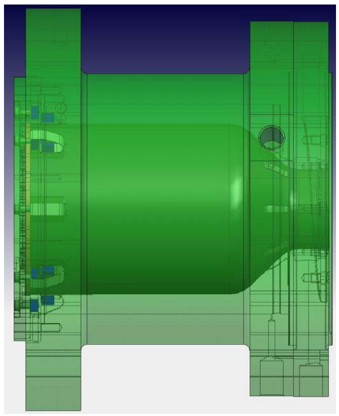

Fig. 14a: Tubular combustion chamber design C 3-2 including attachment systems in assembled state within the test rig

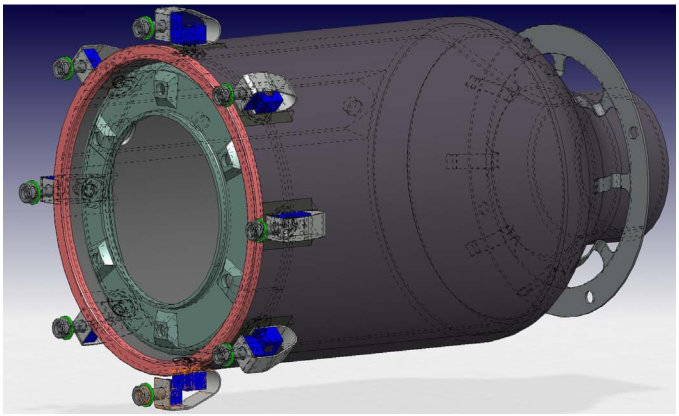

Fig. 14b: Tubular combustion chamber design C 3-2 including attachment systems showing the upstream metallic attachment system and the rear metallic spring element

As a consequence, the design concept C 3-1 uses integral manufactured CMC brackets, which are attached to the upstream flange of the test rig via metallic brackets. In doing so, the attachment system is flexible in the radial direction, but having a relatively high stiffness in the lateral direction leading to a defined condition of the installed combustion chamber. In contrast to this the downstream metallic spring element is flexible in both directions (radial and lateral) enabling the CMC combustion chamber to expand due to the emerging temperatures. The experiences on CMC adequate design including metallic attachment systems reveals, that for the bolted connection of the upstream attachment system (at the interface CMC bracket - metallic bracket) special thermal stress-free fasteners should be used compensating the mismatch of thermal expansion coefficients effectively [24].

The difference to the second design concept C 3-2, depicted in Figures 14a and 14b, can mainly be attributed to the upstream attachment system.

Thereby the combustion chamber is characterized by a "clean" tubular CMC design, i.e. no integral CMC brackets are needed, having the advantage of an eased manufacturing and elevated robustness. The outer bypass of the metallic bracket of the upstream attachment system further leads to an elevated radial flexibility. The rear spring element is in accordance to the C 3-1 design.

Although FEM structural analysis can verify the feasibility of the design comparably fast, technology samples and manufacturing trials are essential in order to enable an early and profound consolidation of the design. These manufacturing trials can comprise adequate components for investigations on spring-back and shrinkage effects or can relate to manufacturing parameters e.g. for the application of EBC coatings and for the introduction of cooling channels. Moreover, specific technology samples and sub-element testing are envisaged, in order to evaluate degradation effects of cooling channels on the mechanical performance of oxide

CMC. Although the combustion chamber is designed for the given test rig corresponding conditions are similar to true gas turbine environments and the verification of design features such as CMC composition, lay-up, and attachments systems can most suitably be performed. Throughout these developments also the spin-off related to the use of oxide CMC for TPS and HS applications is of elevated interest for ASTRIUM Space Transportation in particular for reusability.

2.1.2 Segmented Design

In order to minimize strain transfer to the CMC components, the DLR Institute of Structures and Design designed a self-adapting attachment concept that automatically compensates the differences of thermal expansion. Furthermore, for limiting cost of testing, the three developed oxide CMCs would be mounted together in one prototype and then tested during a same test campaign.

In the developed combustor concept, the CMC combustor liner is segmented in three parts and is intended to be fixed in the metallic housing. The combustor prototype is composed of single curved CMC segments bolted together at radially oriented metallic brackets (Figure 15). These brackets contact the inner face of the housing. Through adapted thickness and form, the six metallic brackets bring elasticity to the combustor structure and assure vibrations damping during the test phase. Another advantage is the self-positioning in radial direction of the CMC structure in the housing. Additionally, the radial motion of the three segments is compensated at their rear end through an attachment system. Via the designed concept, both structures, the CMC liner and the metallic housing, are able to radially expand almost freely at any service temperature.

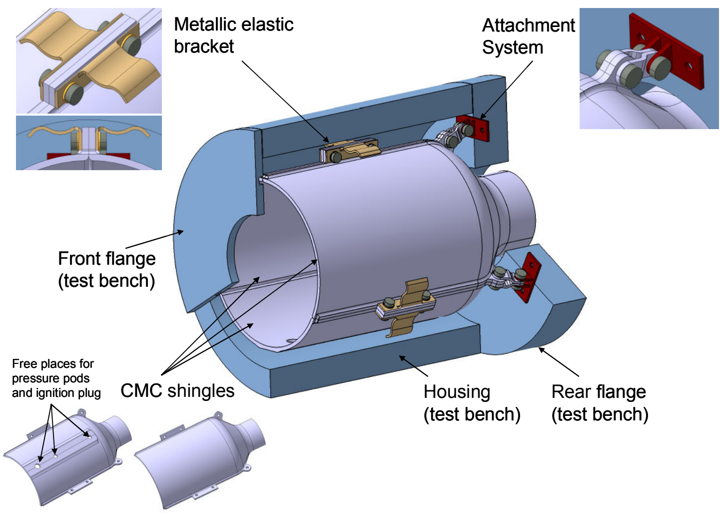

Fig. 15: Fixation concept of the CMC segmented combustor prototype

The DLR Institute of Structure and Design is also responsible for the dimensioning of the combustor segments on the basis of realistic loads and environmental conditions. The temperatures in the wall segments calculated via conjugate heat transfer simulation described in section 2.1.3 by the DLR Institute of Propulsion Technology, are interpolated into a FEM (Finite Element Method) simulation model, with which the induced stresses in the segments can be determined.

As a first approach, a preliminary periodic 3D model was simulated with the FEM software ANSYS. The model represented a 1/124 part of a cylindrical combustor liner. The effusion cooling holes were geometrically modeled. As the fixation concept should allow free radial displacement of the CMC components, following boundary conditions are applied: periodic boundary conditions on the frontier of the periodic part, thus the hoop displacement is constrained and fixation of the axial displacement on one outer face.

The simulated material was WHIPOX with a winding angle ±30° in hoop direction, an alumina matrix and fibers Nextel 610 (3000den). Material data measured by Advanced Ceramics Bremen and presented in section 1.4 were used. The material was modeled as orthotropic and with solid elements. Temperatures resulting from heat transfer analysis with cooling consideration (see section 2.1.3) were interpolated on the FEM mesh. The pressure difference in the wall, allowing a cooling film formation, was modeled with a pressure of 1.65bar applied on the outer face of the combustor. A static structural analysis is then performed. The maximum stress criterion was used:

$$\sigma_{principal} < \frac{Strength}{Factor\_of\_Safety}$$

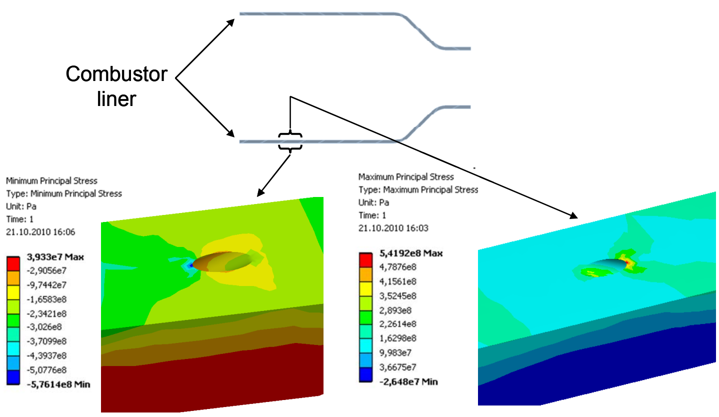

Fig. 16: Maximal and minimal principal stresses calculated on the WHIPOX combustor liner

The modeled WHIPOX strip can deform almost freely, thus the stresses were mainly induced by the temperature gradients in the CMC liner. Temperatures between 961K and 1303K induced a maximal axial deformation of 1.5mm and a radial deformation between 0.17 and 0.46mm. Higher values of maximal and minimal principal stresses (respectively tensile and compressive stresses) appeared at the edges of the cooling holes (Figure 16), mainly in the direction of fiber reinforcement.

In an earlier DLR internal project, flat CMC wall elements were tested on a combustor test bench; in parallel the parts were analyzed with coupled computational fluid dynamics (CFD) and FEM analyses. It was shown that the local calculated stresses near the cooling holes did not induce a failure of the component. This first simulation pointed out the critical regions of the model and enhanced the planning of the next simulation steps. Further, the combustor with its attachment system will be simulated using FEM analyses in later studies. This will be supported by the use of realistic temperatures resulting from CFD analyses. Additionally, local FEM analyses of attachment systems in parallel to real testing of attachment systems will enhance the understanding of the fixation concepts.

2.1.3 Cooling development and testing

Within the HiPOC project numerical investigations are carried out to design the cooling concepts. Design calculations of the liner for a tubular demonstrator combustor are shown as an example, Figures 17 and 18. A conjugate heat transfer problem was solved, where the influence of turbulent heat transfer due to convection from the hot gases to the wall, heat conduction in the solid parts, as well as radiation were considered. The open source CFD-tool Code Saturne in combination with the thermal FEM code Syrthes for conduction/radiation problems was used for the calculation [25]. Both codes were coupled after each time step to ensure a consequent and continuous data exchange between the fluid and the solid phase. To enable the calculation with Syrthes a preprocessing step for the solid mesh was needed, because of the specific data structure used in Syrthes.

The calculations were performed for the WHIPOX of 3 mm thickness for the demonstrator liner and a TBC (Thermal Barrier Coating) layer of 1mm thickness that protects the CMC. The temperature dependency of the thermal properties such as heat capacity and thermal conductivity has been accounted for in the calculation. To simplify the problem, only the flow in the combustion chamber was calculated while for the inflow conditions a generic profile of the velocity components was used to simulate an expanding burner flow field. The inflow conditions were generated in such a way, that the hot gases which were set to 2150K at the inflow, directly hit the demonstrator liner to simulate real conditions. The operating pressure is about 55bar. The temperature of the cooling air was set to 961K and the pressure loss over the effusion holes was examined with about 3%. The calculated surface temperature distribution at the front part of the liner is show in Figure 17. The TBC layer is in direct contact with the fluid, whereas the CMC layer is shielded by the TBC layer.

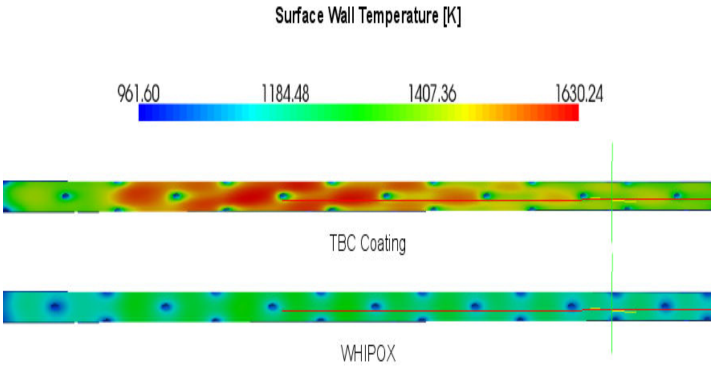

Fig. 17: Surface wall temperature distribution for the TBC and the WHIPOX layer

A maximum temperature of about 1630K was calculated on the TBC surface while the maximum temperature for the CMC is only about 1305K. A starter cooling film is injected to protect the upstream part of the liner because of inefficient effusion cooling in this region. Nevertheless, the liner is heated because of radiative heat transfer. As can be seen in Figure 18, the complete liner wall has been simulated and represents a temperature distribution which is used to calculate the stresses.

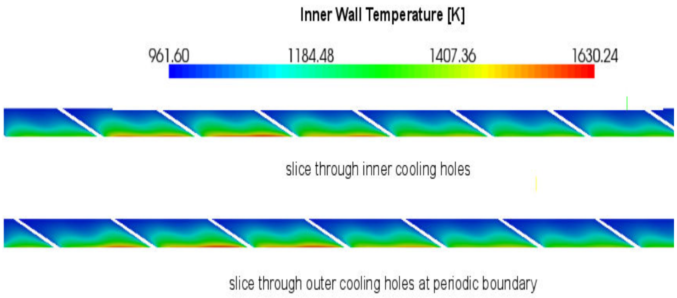

Fig. 18: Inner wall temperature distribution for the liner wall at different longitudinal cross sections

The planar wall elements will be tested in a high pressure cooling test rig. Hot exhaust gas is flowing through a test section with optical access to the hot gas side of the test sample. A detailed description of the test rig is given in [26]. The operating parameters

- Hot gas pressure
- Hot gas temperature
- Hot gas velocity
- Cooling air temperature
- Cooling air pressure drop

can be set independently in order to analyze the influence of the respective parameter on the cooling effectiveness. The wall temperature distribution is measured by an IR-camera. An investigation on the cooling performance of different advanced cooling concepts for metallic walls is described in [27].

2.2 Turbine seal segment

For the development of the seal segment at Rolls-Royce Deutschland, the approach was taken to first search in open literature, also in form of patents. Then two fundamentally different concepts were selected and studied in detail, including stress calculation, optimization and discussion with manufacturing. To baseline the stress calculations, all specimen testing done within the HiPOC program were simulated using an analytical code ALAN developed by IKV [28] and a proprietary RR FEM code specialized in transient thermo-mechanical simulation. The test specimen and the components are modeled in 2D as orthotropic material and in 3D as stack of UD layers. The UD layer definition in terms of strength and stiffness was derived from the laminate test results described above using inverse laminate theory. In the prelim design phase and for optimization, the thermo-mechanical modeling is limited to 2D. But since the design is now converged, 3D FEM models will be generated for both displayed seal geometries within the HiPOC program.

2.2.1 CMC segment around internal carrier

The first basic design concept is a C-shaped cross section held by an internal structure, similar to [29]. It was necessary to modify the cooling concept, as the original idea did not protect the internal metallic carrier from heating up towards the CMC temperature, which is beyond the max operating temperature for the envisioned metal alloy. Finally an air gap insulation with a mix of integral metallic standoffs and ceramic felt buffers was selected in order to allow for the difference in thermal expansion between metal and CMC and still provide a very small air flow between the components in order to stop the heat flux to the metal carrier. The driving pressure for this flow is the pressure difference between the cavities up- and downstream of the seal segment. With a properly sized cooling channel, the pressure drop between seal segment and metal carrier should mimic the pressure drop in the main gas path and minimize thereby the pressure loading on the seal segment. Design and air flow modifications and 2D stress analysis using orthotropic material data was iterated several times, see Fig. 19-21 for the final design. The slight backside cooling as well as the wall and coating thickness was adjusted to achieve a coating peak temperature of 1623K and a CMC peak temperature of 1423K. The radius of the curvature of the CMC segment reaching around the metallic carrier was increased in several steps to reduce fiber bending as well as the thickness of the CMC segment was steadily reduced to minimize the through-thickness temperature gradient. Both modifications lowered the stresses to a level acceptable for the oxide/oxide CMC materials studied in the framework of this program. In Fig. 19, the in-plane stress for a WHIPOX seal segment featuring a ±30° fiber angle relative to the axial direction is shown.

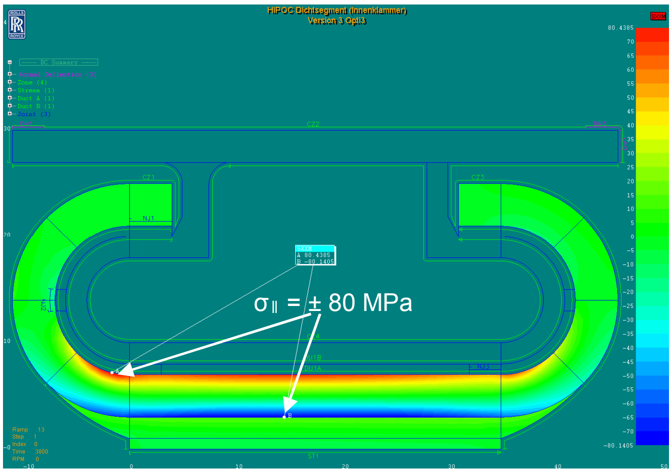

Fig. 19: In plane stress field in geometry 1

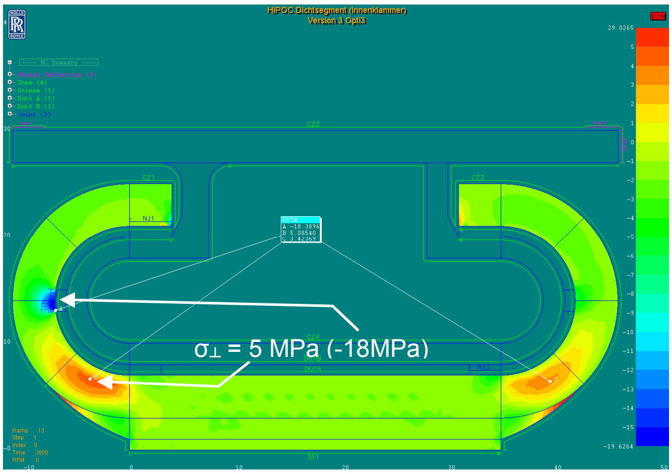

Fig. 20: Out of plain stress field in geometry 1

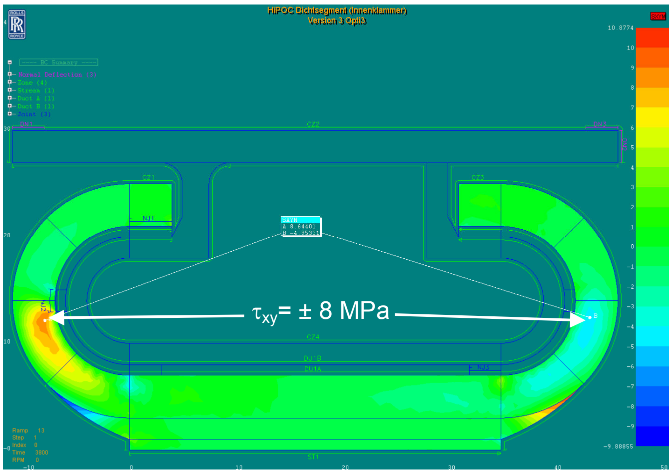

Fig. 21: Shear stress field in geometry 1

Fig. 20 displays the out of plane stress for this configuration. And in Fig 21 the xy shear stress is plotted. The resulting shape of the CMC segment has some similarity to previously published work [30], confirming the approach taken. The dishing (flattening of curvature in circumferential direction) of the seal segment due to the radial temperature gradient will be investigated by 3D thermo-mechanical FE analysis as stack of UD layers. This 3D study will also be used to determine the required properties of the ceramic felt buffers between CMC and metal carrier.

2.2.1 CMC segment in two metal rails

The second basic concept is a flat CMC plate held by two metallic rails at the up- and down-stream end, similar to [31]. This concept requires the metallic rails to be protected from the hot gases of the main gas path. This can be accomplished by the extension of the downstream end of the upstream vane platform and the upstream extension of the downstream vane platform. Due to the thickness required for the structural integrity of these extended platforms, there is a significant difference in radial position of the CMC to metal interface at the rails and the further inboard position of the abradable coating on the CMC potentially getting into contact with the blade tip. If the thickness of the coating should be limited to a value smaller than this difference in radial position, the cross section of the seal segment needs to be changed to an arc instead of a flat plate, see Fig. 22-24 for the final shape. This saddle shaped contour of the CMC should not cause difficulties during manufacturing as the curvature in the circumferential direction has a relatively large radius. The slight backside cooling was again adjusted to achieve a coating peak temperature of 1623K and a CMC peak temperature of 1423K. During several design and 2D stress iterations based on orthotropic material data, the thickness of the CMC segment was steadily reduced as well as the pressure in the cavity behind the segment in order to reduce the stresses to a level acceptable for the available oxide/oxide CMC materials.

Also the square shape of the rails was changed to a gradual thinning of the metal rail at the interface to the CMC, so that the load on the CMC by the internal pressure can deflect the rail, thereby gradually transferring the load from CMC to metal. To prevent the air in the closed cavity to heat up to the full CMC operating temperature during prolonged operation and thereby overheating the metallic carrier, this cavity needs to be vented. Since it is not so easy to generate a pressure gradient along the segment back side in this design, it was decided to reduce the pressure in the cavity as a whole to just slightly above the pressure in the cavity upstream of the seal segment. The resulting pressure difference across the seal segment generates the force, which locates the segment against the metal carrier. Before engine start, the seal segment is located by the up- and downstream sides of the seal segment and the matching surfaces at the metallic carrier allowing for a minimum play in cold build.

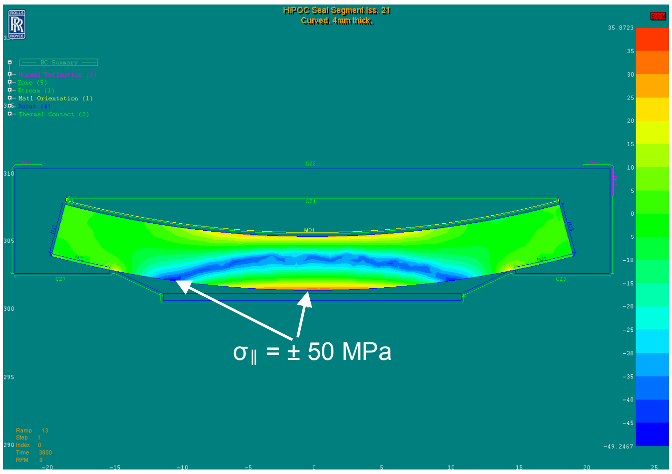

Fig. 22: In plane stress field in geometry 2

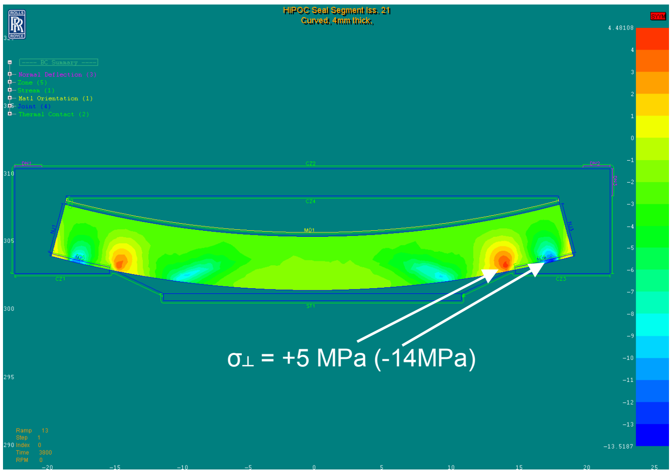

Fig. 23: Out of plain stress field in geometry 2

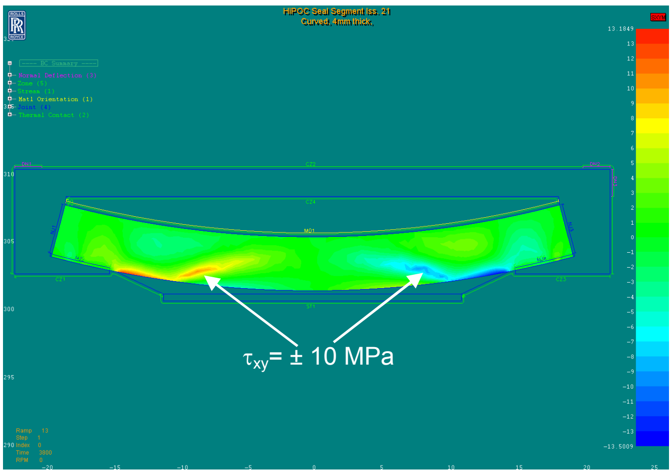

Fig. 24: Shear stress field in geometry 2

In Fig. 22, the in-plane stress of the final design for a WHIPOX seal segment featuring a ±30° fiber angle relative to the axial direction is shown. Fig. 23 displays the out of plane stress for this configuration. And finally, in Fig. 24 the xy shear stress is plotted. The dishing of the seal segment due to the radial temperature gradient will be investigated by 3D thermo-mechanical FE analysis as stack of UD layers. This 3D study will also be used to determine the required thickness and stiffness of the compliant layer between CMC and metal rail.

3. SUMMARY AND PROGRAM OUTLOOK

The CMC materials, WHIPOX, UMOX and OXIPOL have been studied in detail, as documented by room temperature testing. By the end of the program in January 2012, high temperature materials testing will be conducted, including creep studies. Cooling schemes for oxide/oxide CMC have been developed by conjugate heat transfer calculations based on the coupling of a finite volume CFD code for the gas flow with a FEM code for the thermo-mechanical calculation of the combustor wall. These predictions were validated by testing in a dedicated cooling rig at representative temperatures, velocities and density ratios. Further iterations will be carried out until the end of the program in order to fully optimize the effusion cooling scheme for use with low conductivity materials such as oxide/oxide CMCs. Tubular and segmented combustor designs as well as two different seal segment designs have been worked up by iterating design modifications and stress calculations taking manufacturing input into account. After the decision is made between the designs, a combustor for testing in the high pressure single sector test facility of DLR will be manufactured and qualified. Finally, the CMC combustor will be tested with pressure, temperature and air-fuel ratio being representative for an aero engine on a regional airplane. Abradable EBC systems have been studied by cyclic burner rig tests. Promising configurations have been identified and will be tested in a rub-in rig using flat specimens. Further iteration on coating application will be carried out in order to improve the adhesion of the coatings. Manufacturing trials of the seal segment will conclude this activity, as currently no further validation testing on curved seal segments is planned within the HiPOC timeframe. At the end of the program in 2012, the results will be used to update a performance deck of a regional engine to quantify the improvements in terms of specific fuel consumption and CO_2 emission reduction.

ACKNOWLEDGMENTS

This work is part of the HiPOC project (contract number 03X3528) within the WING framework. It is funded in part by the German Federal Ministry of Education and Research (BMBF) and administered by Projektträger Jülich (PTJ). Their support is gratefully acknowledged.

REFERENCES

[1] Koyama, T., Hayashi, S., Yasumori, A., Okada, K., Schmücker, M. , Schneider, H., 1996, “Microstructure And Mechanical Properties Of Mullite/Zirconia Composites Prepared From Alumina And Zircon Under Various Firing Conditions”, J. Europ. Ceram. Soc., 16(2), pp. 231-237.

[2] Hirata, Y., Matsushita, S., Ishihara, Y., Katsuki, H., 1991, “Colloidal Processing And Mechanical Properties Of Whisker-Reinforced Mullite Matrix Composites”, J. Am. Ceram. Soc., 74(10), pp. 2438-2442.

[3] Chawla, K. K., 1998, “Composite Materials: Science And Engineering”, 2nd ed., Springer, New York, pp. 212-251.

[4] Strife, J. R. and Sheehan, J. E., 1988, “Ceramic Coatings For Carbon-Carbon Composites”, Am. Ceram. Soc. Bull., 67(2), pp. 369-374.

[5] van Roode, M., Price, J., Otsuka, J., Szweda, A., More, K., Sun, J., 2008, “25,000-Hour Hybrid Oxide CMC Field Test Summary”, ASME Paper No. GT2008-51379.

[6] Lange, F. F., Tu, W. C., Evans, A. G., 1995, “Processing Of Damage-Tolerant, Oxidation Resistant Ceramic Matrix Composites By Precursor Infiltration And Pyrolysis Method”, Mat. Sci. Eng. A, 195, pp. 145-150.

[7] Göring, J., Hackemann, S., Schneider, H., 2003, “Oxid/Oxid-Verbundwerkstoffe: Herstellung, Eigenschaften und Anwendungen” (in German), in *Keramische Verbundwerkstoffe*, W. Krenkel, eds., Wiley-VCH Weinheim, Germany, pp. 123-148.

[8] Clauß, B. , 2008, “Fibres for Ceramic Matrix Composites”, In *Ceramic Matrix C.omposites*, W. Krenkel, eds., Wiley-VCH Weinheim, Germany, pp. 1-20

[9] Newman, B. and Schäfer, W., 2001, “Processing and Properties of Oxide/Oxide Composites for Industrial Applications” in W. Krenkel, R. Naslain, H. Schneider, eds., *High Temperature Ceramic Matrix Composites*. Wiley-VCH Weinheim, Germany, pp. 600-609.

[10] Motz, G., Schmidt, S, and Beyer, S., 2008, “The PIP-process: Precursor Properties and Applications”, in W. Krenkel, *Ceramic Matrix Composites*, Wiley-VCH Weinheim, Germany, pp. 165-186.

[11] Vogel, W.D. and Spelz, U., 1995, “Cost Effective Production Techniques For Continuous Fibre Reinforced Ceramic Matrix Composites”, in *Ceramic Processing Science and Technology*, 51, pp. 225-259.

[12] Heidenreich, B., Krenkel, W., Frieß, M., 2004, ”Net-Shape Manufacturing Of Fabric Reinforced Oxide/Oxide Components

Via Resin Transfer Moulding And Pyrolysis", Proc. of the 28th Int. Conf. on Advanced Ceramics and Composites B, Ceramic Engineering & Science Proceedings, 25(4).

[13] Denis, S., Frieß, M., Klatt, E., Heidenreich, B., 2010,"Manufacture and Characterization of OXIPOL Based on Different Oxide Fibres", Proc. of the 7th Int. Conf. on HT-CMC, pp. 414 – 419.

[14] Vaßen, R., Traeger, F., Stöver, D., 2004, "New Thermal Barrier Coatings Based on Pyrochlore/YSZ Double-Layer Systems", Int. J. Appl. Ceram. Technol., 1 (4), pp. 351-361.

[15] Traeger, F., Vaßen, R., Rauwald, K.-H., Stöver, D., 2003, "Thermal Cycling Setup for Testing Thermal Barrier Coatings", Adv. Eng. Mater., 5 (6), pp. 429-432.

[16] Steinke, T., Mauer, G., Vaßen, R., Stöver, D., Roth-Fagaraseanu, D., and Hancock, M., 2010, "Process Design and Monitoring for Plasma Sprayed Abradable Coatings", J. of Thermal Spray Technology, 19(4), pp. 756-764.

[17] Behrendt, T., Hassa, Ch., 2008, "A Test Rig for Investigations of Gas Turbine Combustor Cooling Concepts under Realistic Operating Conditions", Proc. IMechE, Part G: J. Aerospace Engineering, 222(G1), pp. 169-177.

[18] Trabandt, U., Ritter, H., Reinkober, H., Schmid, T., Wulz, H. G., 2000, "CMC Large Panel TPS Applied on X-38 Nose Skirt". Proc. of the 30th Int. Conf. on Environmental Systems, SAE Technical Paper Series 2000-01-2234.

[19] Trabandt, U., Handrik, K., 2002, "CMC Nose Skirt Panels for X-38 - Successfully Qualification Tested and Fit-Checked". Proc. of the Second World Space Congress, IAF-No. p.I-7-09IAF, USA.

[20] Knoche, R., Ebeling, W. D., Trabandt, U., 2008, "Thermo-mechanical Design and Plasma Test Verification on PARES CMC Nose Cap". No. 2008-01-2171, Proc. of the 38th Int. Conf. on Environmental Systems, ICES2008, USA.

[21] Knoche, R., Werth, E., Rotärmel, W. , Hald, H., Brach Prever, E., Denaro, A., Langlois, S., 2009, "Thermo-mechanical Design of the IXV Nose Assembly", Proc. of the 6th European Workshop on Thermal Protection Systems and Hot Structures, Germany.

[22] Knoche, R., Werth, E., Goëk, S., Weth, M., 2010, "Thermo-mechanical Design of the ASTRIUM C/SiC Experiment on SHEFEX II", Proc. of the 7th International Conference on High Temperature Ceramic Matrix Composites (HT-CMC7), Germany.

[23] Brewer, D.; Ojard, G. and Gibler, M., "Ceramic Matrix Composite Combustor Liner Rig Test", ASME Paper No. 2000-GT-670.

[24] Wulz, H. G., Stark, H., Trabandt, U., 2000, "Joining and Load Transfer Technology for Hot Structures", AIAA-2000-2435, Proc. of the 34th AIAA Thermophysics Conference, USA.

[25] http://www.code-saturne.org/, 2010

[26] Behrendt, T., Lengyel, T., Hassa, Ch., Gerendas, M., 2008, "Characterization of Advanced Combustor Cooling Concepts Under Realistic Operating Conditions", ASME Paper No GT2008-51191.

[27] Lazik, W., Doerr, Th., Bake, S., v.d. Bank, R., Rackwitz, L., 2008, "Development of Lean-Burn Low-NOx Combustion Technology at Rolls-Royce Deutschland", ASME Paper No. GT2008-51115.

[28] Lambrecht, L., 2010, "Advanced Laminate Analysis (ALAN)", IKV, RWTH Aachen.

[29] Morrison, J., 2004, "Ceramic matrix composite component for a gas turbine engine", US patent no. US6758653.

[30] Corman, G. S.; Brun, M. K.; Luthra, K. L., 1999, "SiC fiber reinforced SiC-Si matrix composites prepared by melt infiltration (MI) for gas turbine engine application", ASME Paper No. 99-GT-234

[31] Marini, B.D., Keller, D.A., Radonovich, D.C., Merril, G.B., Vance, S.V., Schiavo, A.L., 2008, "Ring seal for a turbine engine", US patent application No. US2008/025838.